A Dual Concentric Ring Test for Evaluating Residual Stress Development Due to Restrained Volume Change

Schlitter, J., L.[1], Senter, A., H.[2] Bentz, D. P.[3], Nantung, T.[4], and Weiss, W. J.[5]

Abstract

A new test is being developed to evaluate the performance of concretes undergoing both expansion and shrinkage during hydration and/or temperature changes under mechanically restrained conditions. The standard restrained ring test (ASTM 1581-09) is a simple, economical method to evaluate a concrete mixture's susceptibility to develop shrinkage cracking when it is restrained. Unfortunately, the test only provides restraint against samples that shrink and cannot be used to characterize materials undergoing expansion. Further, the conventional restrained ring test does not apply in cases in which the concrete undergoes large variations in temperature, since the restraint changes dimension under heating and cooling. This paper describes a test that was designed to overcome both of these limitations. The new dual concentric ring test provides restraint for both shrinkage and expansion, and has incorporated the ability to study thermal stresses by using a restraining ring having a very low thermal expansion coefficient. This paper will discuss the design and construction of the test device and will present preliminary data that characterizes its ability to quantify and evaluate restrained expansive, shrinkage, and thermal stresses.

Keywords: Restrained Ring Test, Dual Ring Test, Concrete, Thermal Cracking, Shrinkage, Expansion, Internal curing, Autogenous Shrinkage

[1.] Graduate Research Student, School of Civil Engineering, Purdue University, West Lafayette, IN 47907 (corresponding author) email: jlschlit@purdue.edu.

[2.] Undergraduate Research Student, School of Civil Engineering, Purdue University, West Lafayette, IN 47907 email: asenter@purdue.edu.

[3.] Chemical Engineer, Building and Fire Research Laboratory, National Institute of Standards and Technology, 100 Bureau Dr., Stop 8615, Gaithersburg, MD 20899. E-mail: dale.bentz@nist.gov

[4.] Indiana Department of Transportation, Office of Research and Development, 1205 Montgomery St, West Lafayette, IN, 47906, USA

[5.] Professor, School of Civil Engineering, Purdue University, West Lafayette, IN 47907; e-mail: wjweiss@ecn.purdue.edu.

1.0 Introduction

Cementitious materials undergo volume change at early ages due to chemical reactions, self desiccation, external drying, and thermal changes [1-9]. Residual stress develops in the cementitious material when this volume change is restrained [9-12]. If the residual tensile stress becomes too large, cracking may occur. This cracking is significant as it inhibits otherwise durable concrete from reaching its potential service life by allowing deleterious materials to enter the cracks, thereby accelerating degradation [13, 14]. .

The concerns associated with early-age cracking have spurred the development of many tests to assess a material's cracking potential. Tests based on uniaxial restraint such as cracking frames and temperature-stress testing machines have been implemented by Kovler [15], Springenschmid [16], Lange [17], Marchand [18], and van Breugel [19]. Another common method that has been used to quantify a mixture's performance is the restrained ring method [20]. This approach has been used for nearly a century, and recently the restrained ring test (ASTM C 1581-04) [21] has been standardized as a procedure to assess the shrinkage cracking potential of cementitious mixtures. This test is performed by casting an annulus of a cementitious mixture (paste, mortar, or concrete) around a steel ring. Residual tensile stress is generated in the sample when it attempts to shrink but is restrained by the inner steel ring. A crack results if the residual stress exceeds the developing tensile strength. This is observed to correspond with a sudden drop in the measured strain. Stresses and cracking time in the sample are determined by instrumenting the ring with strain gauges.

The vast majority of concrete used in the field is restrained; however, the extent to which this restraint occurs varies. Slabs-on-grade are restrained by the subgrade, concrete bridge decks are restrained by beams, girders, or abutments and elevated composite slabs are restrained by the structural steel supporting girders. One question when developing a restrained shrinkage test is the level of restraint that should be provided to limit the movement of the concrete. The amount of restraint provided is commonly quantified using a term called the degree of restraint (DOR). The DOR describes the percentage of concrete shrinkage or expansion deformation that is prevented by the restraining elements. When all the deformation of a member is prevented it can be considered to be 100% restrained (i.e., a degree of restraint of 1). Free shrinkage corresponds to a 0% degree of restraint. Partial restraint occurs when the DOR is between 100% and 0%. This partial restraint can be calculated using the geometry and stiffness of the concrete and the restraining element [22, 23].

2.0 Research Significance

The conventional restrained ring test has been widely used to evaluate the restrained shrinkage cracking potential of concrete mixtures but is limited in two significant ways. First, the test can only measure net shrinkage due to its configuration where expanding samples come out of contact with the restraining ring. This limitation becomes significant when studying expansive cements [24], shrinkage reducing admixtures [25], and internal curing [26] as these technologies may result in early age expansion. The second limitation of the restrained ring test is that it

must operate at a constant temperature since the ASTM A53 Grade B steel pipe that is typically used for the restraining rings will expand or contract if the temperature changes. As a result, a temperature change would alter the level of restraint experienced by the cementitious annulus.

This paper proposes a test method that can evaluate materials that may expand and that can operate while varying temperature. This test, called the dual concentric ring test, uses two concentric restraining rings; one on the outside of the sample and one on the inside of the sample. This enables restraint in both expansion and contraction and measurement of the strain in the restraining elements as samples shrink and expand. The rings are constructed from Invar, a metal with an extremely low coefficient of thermal expansion that allows the temperature to be varied without dramatically altering the degree of restraint. This enables the study of thermally induced volume changes in addition to volume change from autogenous shrinkage. A wide variety of temperature profiles can be selected to simulate most field conditions. The ability of the test to induce thermal residual stresses has the potential to quantify the restrained cracking capacity of a mixture at any desired time. This can lead to an approach where a mixture could be tested multiple times in the dual ring and purposely cracked at various ages with temperature reduction to develop a cracking curve.

3.0 Experimental Equipment

3.1 Restraining Ring Material and Geometry

The restraining rings were fabricated from an Invar Steel alloy instead of conventional ASTM A53 Grade B steel (used for the standard ASTM C 1581-09 single ring test) in order to minimize the effects of temperature variation on the degree of restraint. Invar is a steel nickel alloy with a coefficient of thermal expansion (CTE) at or less than 1.3×10^{-6} ε/°C [27-29], compared to 12.0×10^{-6} ε/°C for conventional steel [30]. For reference, the coefficient of thermal expansion of early age mortar varies [31-33], but is typically within the range of 8×10^{-6} ε/°C to 10×10^{-6} ε/°C. The thermal deformation of the restraining ring directly affects the degree of restraint of the sample during a temperature change. Larger restraining ring CTE values will produce a greater reduction in the degree of restraint which results in less residual stress development in the sample. This effect is significant because studying the restrained thermal behavior of the sample relies on developing residual stress in the sample during a temperature change. The lower CTE of an Invar restraining ring overcomes this limitation by stabilizing the degree of restraint during a temperature change and allows residual stress to be induced and measured.

The dual ring geometry is presented in Figure 1 where R_{OC} and R_{IC} are the outer face and inner face radii of the specimen respectively, R_{OO} is the outer face of the outer restraining ring radius, R_{II} is the inner face of the inner restraining ring radius, and t is the thickness of each restraining ring. The dimensions are as follows: R_{OC} = 203 mm ± 3 mm (8.0” ± 0.12”), R_{IC} = 165 mm ± 3 mm (6.5” ± 0.12”), R_{OO} = 222 mm ± 3 mm (8.75” ± 0.12”), R_{II} = 146 mm ± 3 mm (5.75” ± 0.12”), t = 19 mm ± 3 mm (0.75” ± 0.12”), and 76.2 mm ± 3 mm (3” ± 0.12”) tall. The measured weight of the inner ring is 11.5 kg (25.4 lb) and that of the outer ring is 16.0 kg (35.2 lb).

It should be noted that the thickness of the restraining ring is slightly different than the current ASTM standard. This difference is intentional since the elastic modulus of Invar© E_{INVAR}=141 GPa (20450 ksi) [27] is less than that of the conventional steel, E_{STEEL}=200 GPa (29000 ksi). As a result, an Invar ring of the same size as the standard steel ring would provide less restraint to shrinkage. The goal of the design of the ring for this study was to match the degree of restraint of the dual ring to that of the conventional ASTM C 1581-09 restrained ring test. The degree of restraint of a restraining ring can be calculated by Equation 1 [22]:

$$\Psi = 1 - \frac{E_c}{E_s} \cdot \frac{1}{\frac{E_c}{E_s} - \frac{1 - \left(\frac{R_{II}}{R_{IC}}\right)^2}{1 - \left(\frac{R_{OC}}{R_{IC}}\right)^2} \cdot \frac{\left[\left(1+\upsilon_c\right)\cdot\left(\frac{R_{OC}}{R_{IC}}\right)^2 + \left(1-\upsilon_c\right)\right]}{\left[\left(1+\upsilon_s\right)\cdot\left(\frac{R_{II}}{R_{IC}}\right)^2 + \left(1-\upsilon_s\right)\right]}} \quad (1)$$

where E_c represents the elastic modulus of the cementitious mixture, E_s represents the elastic modulus of the ring metal, ν_c represents Poisson's ratio for concrete, ν_s represents Poisson's ratio for the ring metal, and Ψ is the degree of restraint. In order to compare ring geometries, the modulus of elasticity and Poisson's ratio for the sample were assumed as constant values of E_c = 32 GPa (4641ksi), and ν_c = 0.18. Poisson's ratio for both the steel and Invar were selected as ν_s = 0.3.

Figure 2 shows the relationship between the Invar ring thickness and the degree of restraint calculated with Equation 1 and the above mentioned specimen values. The degree of restraint increases as the restraining ring is thickened. The Invar ring thickness that corresponds to a degree of restraint equal to that of the ASTM C 1581-09 (72%) was found to be 19 mm.

3.2 Instrumentation and Data Acquisition

The stress that develops within the cementitious sample is determined by measuring the strain in the Invar rings. Both of the Invar rings were instrumented with four opposing CEA-00 series strain gauges [34] that were mounted at mid height. Figure 1 illustrates gauge locations. The inner ring gauges were installed at mid height on the inner face of the inner ring while outer ring gauges were installed at mid height on the outer face of the outer ring. All gauges are operated as shunt calibrated quarter bridge circuits. The gauges have a grid resistance equal to 120 % ± 0.3% Ω, Gage Factor 2.05 % ± 0.5 % at 24 ˚C, temperature correction of Gage Factor +1.2 ± 0.2, and an operating temperature range of -75 ˚C to +175 ˚C [34].

The gauges were installed with a Vishay© installation kit [35, 36]. Each mounting area was sanded smooth and cleaned with an acidic solution. After neutralizing the area treated with acid, the gauges were installed with M-Bond-200 modified alkyl cyanoacrylate adhesive. The

gauges were covered with Teflon tape, butyl rubber sealant, neoprene rubber, and sealed with aluminum tape. Strain relief folds were applied to the gauge lead wires.

A Vishay© system 5000 data scanner paired with Strain Smart© software was used to automatically record strain gauge data at five minute intervals. Data recording initiates immediately after the specimen is sealed in the insulation chamber which typically occurs about 30 min after water contacts cement during mixing.

3.3 Strain Gauge Temperature Calibration

General practice shows that output from bonded strain gauges can change significantly when exposed solely to a temperature change [37, 38]. This is caused by the concurrent effects of changes in the gauge's grid resistivity and the mismatch in thermal expansion coefficients between the strain gage and substrate (in this case the ring). Therefore, even though the Invar ring dimensions are nominally stable throughout the test's temperature range, the gauges still require thermal correction. It should be noted that the gauges used in this test are specifically designed for use on substrates with low thermal coefficients to minimize error caused by temperature change. Several methods are available to correct thermal output with varying degrees of confidence and accuracy. First hand corrective measurement was chosen to correct the dual rings because it is the most accurate method of thermal correction as it accounts for many gauge specific issues [37, 38]. This involved generating a correction curve for each gauge by varying the temperature of the rings in the unstressed state and recording the resulting output. Figure 3a and Figure 3b illustrate the strain correction curves for gauges on the inner and outer rings, respectively. It should be noted that the curved shape of the plot is expected and is typical [37]. Strain Smart© has a function that corrects the strain output based on these curves from temperature readings taken on the ring surface. This is accomplished by taping a type T twisted pair thermocouple to the surface of the ring. Since the thermal uniformity of the rings is high, as discussed later in this paper, it is not necessary to measure temperature at every strain gauge. The correction curves were verified by subjecting the rings to a temperature change without a sample. Figure 3c illustrates the corrected output, and it can be seen that once the correction is applied the gauge output varied less than 4 $\mu\varepsilon$ when subjected to a 45 $^{\circ}$C temperature change.

3.4 Insulating chamber

An insulation chamber was constructed to control temperature and provide options for semi-adiabatic studies. Figure 4a shows the general view of the test setup in the insulation chamber. The restraining rings rest on a circular section of plywood base lined with an acetate sheet to provide a sealed, low friction surface. Four eye bolt lugs mounted to the base allow the assembly to be lifted in and out of the chamber. The rings are surrounded on all sides by a minimum of 50 mm (2") thick microporous insulation with a thermal conductivity of 0.019 W/m·K

at 20 °C (approximately half that of conventional glass fiber insulation). The top portion of insulation is removable to provide access to the chamber.

3.5 Temperature Control System

Temperature control is provided via a programmable 28 liter water bath system pumping an ethylene glycol water mixture at 24 liters/min through a looped copper coil inside the chamber. The ethylene glycol mixture enables the bath temperature to be lowered below freezing to approximately -20 °C. Figure 4b shows the placement of this coil on top of the restraining rings. A circular 3.2 mm (1/8") thick sheet of aluminum is placed on top of the rings to provide a rigid platform for the coil. The water bath continuously monitors the temperature delivered to the chamber by using an external probe mounted on the inlet of the coil. This enables the system to automatically compensate for heat loss or gain through the tubing connecting the bath to the chamber. In-line valves are installed on the external tubing to allow the user to turn the coil flow on or off.

The system's heating and cooling capabilities were determined by placing four type T thermocouples on an aged mortar sample at room temperature and varying the bath temperature as quickly as possible. The heating test targeted an end temperature of 50 ˚C and it can be seen in Figure 5a that the maximum temperature change the system can generate is about 1.8 ˚C per hour at a 20 degree differential between the bath and sample. The cooling test targeted an end temperature of 13 ˚C as shown in Figure 5a. It can be seen the temperature change rate decreases as the difference between bath and sample temperature decreases. The maximum thermal differential recorded in the sample during forced heating and cooling between two points spaced vertically or horizontally on the ring was 0.3 ˚C. This indicates that forced heating and cooling produces uniform temperatures in the sample.

4.0 Semi Adiabatic Properties of Chamber

The insulating properties of the chamber were examined by heating or cooling a well aged mortar sample with the coil and then allowing it to naturally return to ambient room temperature. The resulting temperature change was monitored with a type T thermocouple embedded in the sample. Figure 5b illustrates the free heating and cooling curves of the sample in the chamber. It can be seen, similar to forced heating and cooling, a larger temperature difference between the sample and ambient air will produce a faster temperature reduction or increase.

The heat transfer coefficient of the system was determined to quantify effectiveness of the insulation chamber and to provide a method to extrapolate the measured semi-adiabatic case to a theoretical adiabatic condition. First the amount of heat flowing into or out of the chamber was calculated from the free heating and cooling thermal profiles and Equation 2:

$$Q = (M_{RINGS}C_{p\_RINGS} + M_{SAMPLE}C_{p\_SPECIMEN})\Delta T \quad (2)$$

where Q represents the total heat flow (kJ), M_{RINGS} is the combined mass of the two Invar rings (27.5 kg), M_{SAMPLE} is the mass of the sample (1.7 kg), C_{P_RINGS} is the heat capacity of Invar (0.460 kJ/kg/˚C), C_{P_SAMPLE} is the heat capacity of concrete (1.00 kJ/kg/˚C) and ΔT (˚C) is the change in sample temperature over a 10 hour interval. Total heat transfer was calculated as -54.1 kJ for the free cooling curve and 16.3 kJ for the free heating curve.

Once the heat flow was determined, the heat transfer coefficient was calculated with Equation 3:

$$U = \frac{Q}{A(T_{SAMPLE} - T_{AMBIENT})\Delta t} \quad (3)$$

where U represents the heat transfer coefficient in units of W/m^2/K, A is the measured surface area of insulation exposed to the inner chamber holding the rings/sample (0.511 m^2), T_{SAMPLE} is the temperature of the sample at an instant in time, $T_{AMBIENT}$ is the ambient air temperature outside of the chamber, and Δt is the duration of time in seconds. The resulting heat transfer coefficient was approximately 0.03 W/m^2/K and provides reasonable agreement with the given thermal conductivity of the insulation and its thickness.

In addition to investigating the heating and cooling recovery characteristics of the chamber, the early age semi-adiabatic behavior of a fresh mortar was determined. A mixture designated as M-0 (as detailed later in Table 1) was allowed to freely heat and cool in the chamber and was instrumented with type T thermocouples to determine its thermal history and uniformity. The temperature at four points within the chamber was monitored for five days. Three thermocouples were equally spaced around the ring and embedded in the top quarter of the sample. One thermocouple was placed directly beneath the sample. A fifth monitored the room ambient air temperature. The results of this test are illustrated in Figure 5c, and it can be seen that the maximum difference between thermocouples inside the chamber was only 0.2 ˚C, indicating a high degree of thermal uniformity throughout the sample. The temperature peaked at 38.8 ˚C ± 0.5 ˚C at an age of 20 h and then began cooling towards room temperature. As expected, the cooling curve closely matches the free cooling curve in Figure 5b.

5.0 Materials and Experimental Procedures

5.1 Mixture Proportions

Three mortar mixtures with varying shrinkage performance were chosen to study several capabilities of the dual ring test. They are designated M-0, M-11, and M-24 with their proportions provided in Table 1. M-0 was a plain mortar while M-11 and M-24 utilized internal curing with pre-wetted fine lightweight aggregate (FLWA). All mixtures had a water-to-cement ratio of 0.30 by mass (*w/c* = 0.30) and a paste volume of 45 %. The internally cured mixtures M-11 and M-24 had 11 % and 23.7 % of the total mixture volume comprised of FLWA, respectively. It should be noted the 23.7 % replacement value corresponds to the theoretical value of internal curing water that is required to match the chemical shrinkage [39].

Table 1 - SSD Mixture Proportions

Material	M-0 Plain Mortar (kg/m^3)	M-11 FLWA (kg/m^3)	M-24 FLWA (kg/m^3)
Cement (Type I)	728	728	728
Water	218	218	218
Fine Aggregate	1444	1133	821
FLWA (SSD)	0	204	409

5.2 Materials

Type I ordinary portland cement was used (ASTM C 150-05) with a Blaine fineness of 370 m^2/kg, and an estimated Bogue composition of a 56 % C_3S, 16 % C_2S, 12 % C_3A and 7 % C_4AF. Normal weight river sand was used with a fineness modulus of 2.71 and an oven dry specific gravity of 2.58. The lightweight aggregate used in M-11 and M-24 was a manufactured rotary kiln expanded shale with a fineness modulus of 4.3, an oven dry specific gravity of 1.56, and a 24 hour absorption value of 10.5 % by mass. A high-range water-reducing admixture (HRWRA) was added at a rate of 1 g mass per 100 g of cement. Mix water consisted of tap water conditioned to 23 ˚C ± 1˚C.

5.3 Mixing Procedure

Aggregate for each mixture was batched in the oven dry state. FLWA was presoaked for 24 h ± 0.5 h in the mix water (including the water for prewetting) while sealed in a container. Mixing was performed in accordance with ASTM C 192-07. First aggregate was loaded into the "buttered" mixer. Where applicable, the mixing water was decanted from the FLWA. The mixer was started and 50% of the total water was added. The cement and remaining mix water containing the HRWRA were then added. The mortar was mixed for 3 min, then rested for 3 min while the sides of the mixer were scraped, then mixed for a final 2 min.

5.4 Unrestrained Linear Autogenous Deformation – Corrugated Tube Protocol

Linear autogenous strain of each mortar was measured using a technique where the fresh mortar was placed in corrugated polyethylene molds per ASTM C 1698-09 [40]. The corrugations in the mold produce greater stiffness in the radial direction than the longitudinal thereby forcing shrinkage to occur along the length of the tube. This technique is designed to minimize restraint and yields the free shrinkage profile of each mixture. The single laboratory precision stated in the standard for mortar samples is 28 με.

Each mortar mixture was cast into two corrugated tubes, vibrated, capped, and placed in the dilatometer. Length change of each tube was measured with two linear variable differential transformer (LVDT) displacement transducers and was recorded by the data acquisition system at 5 minute intervals. The recorded values were zeroed to the time of final set as determined by ASTM C 403-08.

5.5 Restrained Shrinkage – Dual Ring Test

The instrumented rings were prepared by coating the surfaces that would make contact with the sample with form release and a layer of acetate sheet in order to minimize friction on the sample. The fresh mortar was then cast between the two rings in two layers. A handheld vibrator was used to consolidate each layer. The top of the sample was struck level with the top of the ring and then capped with the separator plate and temperature control coil. The top layers of insulation and chamber cap were then installed to effectively seal the specimen in the chamber to control its temperature and to prevent drying shrinkage.

The temperature control system was operated at 23 ˚C ± 0.2 ˚C for a minimum of 8 h prior to casting, to bring the rings and chamber to a consistent temperature. It then operated at 23 ˚C ± 0.2 ˚C until the test ended due to the sample cracking or 8 d. After 8 d, the temperature was reduced at a rate of 1˚C/h, to attempt to induce a crack in the sample by utilizing thermal shrinkage to produce additional tensile stress. The minimum temperature applied to the sample in this study is -5 ˚C ± 0.2 ˚C.

The strain measured on the inner ring (ε_{IN}) and outer ring (ε_{OUT}) is reported as the average output of the four gauges on each ring. The precision of the average strains from subsequent tests of the same mixture deviated less than 6 με. These strains can be used to determine the time of cracking by observing a sudden drop in readings. In addition, they can be used to calculate the residual stress that develops in the sample [24, 26]. First the pressure exerted by the sample on the inner ring P_{IN} can be calculated using Equation 4 [22]:

$$P_{IN} = -\varepsilon_{IN} \cdot E_{INVAR} \cdot \left(\frac{R_{IC}^2 - R_{II}^2}{2 \cdot R_{IC}^2} \right) \tag{4}$$

The pressure exerted by the sample on the outer ring P_{OUT} is calculated by Equation 5 [22]:

$$P_{OUT} = \varepsilon_{OUT} \cdot E_{INVAR} \cdot \left(\frac{R_{OO}^2 - R_{OC}^2}{2 \cdot R_{OC}^2} \right) \tag{5}$$

The two pressures obtained from ring strains are then used to calculate the circumferential "residual" stress in the sample at R_{IC} ($\sigma_s(R_{IC})$) by Equation 6a:

$$\sigma_\theta(R_{IC}) = P_{IN} \cdot \left[\frac{R_{OC}^2 + R_{IC}^2}{\left(R_{OC}^2 - R_{IC}^2 \right)} \right] - P_{OUT} \cdot \left[\frac{2 \cdot R_{OC}^2}{\left(R_{OC}^2 - R_{IC}^2 \right)} \right] \tag{6a}$$

Substituting Equations 4 and 5 into 6a yields Equation 6b for the ring geometry employed in this study. The residual stress (σ_θ) is output in units of MPa or PSI when units of MPa or PSI are used in the E_{INVAR} terms. The values for ε_{IN} and ε_{OUT} are input as actual strain.

$$\sigma_\theta(R_{IC}) = -0.58\varepsilon_{IN}E_{INVAR} - 0.58\varepsilon_{OUT}E_{INVAR} \tag{6b}$$

6.0 Results and Discussion

6.1 Results of Unrestrained Shrinkage Test

The unrestrained shrinkage history of the three mixtures during the first 7 days is shown in Figure 6. It can be seen that the plain mortar M-0 shrinks significantly more than the two mixtures M-11 and M-24 that contain the prewetted LWA (internal curing). The M-11 and M-24 mixtures undergo an initial expansion which has been seen by other researchers [41, 42]. After the expansion phase, M-11 begins to shrink while M-24 continues to expand. It should be noted that even though the M-11 mixture shrinks, it does not develop negative strain (tensile).

6.2 Results of Dual Ring Test

The inner and outer ring strain history is illustrated in Figures 7a and 7b, respectively. Residual stress development is shown in Figure 8. It can be seen the plain mortar M-0 only develops strain in the inner ring, indicating that it only shrinks. This was anticipated as the free shrinkage curves only exhibit shrinkage. M-0 continues shrinking until it develops a stress of 3.6 MPa (tension) at approximately 4 d, at which time it cracks.

Mixture M-11 develops no expansive stress and develops a residual tensile tress of 1.4 MPa at 8 d while operating at constant 23 ˚C ± 0.2 ˚C. The temperature was then decreased at a rate of 1˚C/h and the resulting increase in residual stress can be seen until the sample cracks at 3.6 MPa at 8.2 d (14.3 ˚C). This indicates that the samples restrained shrinkage only developed 39 % of the stress required to induce cracking. Also, approximately 6 με of ring strain or 0.2 MPa residual stress in the sample is generated per 1˚C of temperature change.

It can be seen that mixture M-24 develops a slight expansive strain in the outer ring shortly after the measured time of set of 6 h. The expansion peaks at 4 με or 0.15 MPa at 11.8 h and then decreases over a period of 7 h, without producing an opposing reaction on the inner ring. It is likely that this reduction in stress is due to stress relaxation while the modulus of elasticity is low and the creep is high in the sample at early age. Neither shrinkage nor expansion is observed for the remainder of the test while temperature is held at a constant 23 ˚C ± 0.5 ˚C. The free shrinkage history during this time shows a subtle expansion which may not be large enough to overcome the rate of creep under restrained conditions. After approximately 8 d, the temperature in the sample is decreased at a rate of 1˚C/h and an increase in shrinkage strain and residual tensile stress is observed. It can be seen that the rate of ring strain and residual stress development is the same in both the M-11 and M-24 samples. The M-24 sample does not generate a crack by the time it reaches the minimum temperature limit of -5 ˚C.

Relative cracking potentials of M-11 and M-24 can be determined by comparing the amount of additional residual stress required to crack the sample by decreasing temperature. The M-11 sample required an additional 2.2 MPa of tensile stress to induce cracking, while M-24 requires

at least 3.0 MPa since it did not crack. Therefore it can be concluded that M-11 would have a greater potential to crack than M-24. This can be attributed to the amount of tensile stress in the sample immediately before the temperature begins to decrease. Since the M-11 sample begins the cooling period with approximately 1.5 MPa of tensile stress more than that of M-24, it is closer to its cracking capacity. While the slight early age expansion is generally more desired than shrinkage as seen in the M-24 sample, it can be seen that the volume stability of the sample after 12 h has a greater contribution to reducing cracking potential.

7.0 Conclusions

This paper has described the development of a 'Dual Concentric Ring Testing Device' that enables the residual stress that develops in concrete rings to be quantified as concrete expands and contracts due to chemical reaction, hygral shrinkage, or thermal movements. The ring is designed to provide a similar degree of restraint when compared with the ASTM C 1581-09 standard test geometry; however conceptually any geometry can be used.

This paper quantifies the uniformity in temperature that may be expected throughout the ring and indicates that heating and cooling take place with less than 0.2 ˚C variance across extreme points on the sample.

The semi-adiabatic overall heat transfer coefficient for the insulation chamber containing the rings and a typical mortar specimen was calculated as approximately 0.03 $W/m^2/K$.

The results of cooling a sample indicate that when a temperature reduction is added to autogenous shrinkage it may result in cracking, while autogenous shrinkage on its own may not. This may become a useful method to quantify the reserve cracking capacity of mixtures at a desired age. The direct comparison of crack resistance capacity at specific points in time may enable future research to set benchmarks for cracking performance.

The results from testing show that the dual ring can quantify the behavior of residual compressive stress during early age expansion. Restrained early age expansion results in compressive stresses in the sample. These stresses disappear by 24 h. As a result, the shrinkage performance of the sample after 24 h has a greater effect on cracking potential.

8.0 Acknowledgements

This work was supported in part by the Joint Transportation Research Program administered by the Indiana Department of Transportation and Purdue University through Project SPR-3211. The contents of this paper reflect the views and the accuracy of the data presented herein, and do not necessarily reflect the official views or policies of the Indiana Department of Transportation, nor do the contents constitute a standard, specification, or regulation.

9.0 Disclaimer

Certain commercial equipment, instruments, or materials are identified in this report in order to foster understanding. Such identification is not intended to imply recommendation or endorsement by the National Institute of Standards and Technology nor Purdue University, nor is it intended to imply that the materials or equipment identified are necessarily the best available for the purpose.

10.0 References

1. Le Chatelier H. Sur les changements de volume qui accompagnent le durcissement des ciments. Bulletin de la Societe d'Encouragement pour l'Industrie Nationale. 1900:54-7.
2. Neville HA, Jones HC. The study of hydration changes by a volume-change method. Lehigh University -- Publication. 1929;3(1):309-18.
3. Lynam CG. Growth and movement in Portland cement concrete. London, England: Oxford University Press; 1934.
4. RILEM Commission -C. Properties of set concrete at early ages (state of the art report). Mate´r Const. 1981;84 399–460.
5. Powers TC. A discussion of cement hydration in relation to the curing of concrete. Proc Highw Res Board. 1947;27 178–88.
6. Wiegrink K, Marikunte S, Shah SP. Shrinkage cracking of high-strength concrete. ACI Materials Journal. 1996;93(5):409-15.
7. Shah SP, Weiss WJ, Yang W. Shrinkage cracking - can it be prevented? Concrete International. 1998;20(4):51-5.
8. Aitcin P-C, Neville AM, Acker P. Integrated view of shrinkage deformation. Concrete International. 1997;19(9):35-41.
9. See HT, Attiogbe EK, Miltenberger MA. Potential for restrained shrinkage cracking of concrete and mortar. Cement, Concrete and Aggregates. 2004;26(2):123-30.
10. Igarashi S-I, Bentur A, Kovler K. Autogenous shrinkage and induced restraining stresses in high-strength concretes. Cement and Concrete Research. 2000;30(11):1701-7.
11. Altoubat SA, Lange DA. Creep, shrinkage, and cracking of restrained concrete at early age. ACI Materials Journal. 2001;98(4):323-31.
12. Radlinska A, Bucher B, Weiss J. Comments on the interpretation of results from the restrained ring test. Journal of ASTM International. 2008;5(Copyright 2009, The Institution of Engineering and Technology):JAI101944 (12 pp.).
13. Wang K, Shah SP. Permeability study of cracked concrete. Cement and Concrete Research. 1997;27(3):381-93.
14. Weiss J. Prediction of Early-Age Shrinkage Cracking in Concrete Ph.D. Dissertation. Evanston, IL, Northwestern University; 1999.
15. Kovler K. Testing system for determining the mechanical behaviour of early age concrete under restrained and free uniaxial shrinkage. Materials and Structures. 1994;27(6):324-30.
16. Springenschmid R, Breitenbucher R, Mangold M. Development of the cracking frame and the temperature-stress testing machine. In: Proceedings of the International RILEM Symposium: Thermal Cracking in Concrete at Early Ages1994. p. 137–44.
17. Altoubat SA, Lange DA. Creep, shrinkage, and cracking of restrained concrete at early age. ACI Materials Journal. 2001;98(Compendex):323-31.
18. Pigeon M, Toma G, Delagrave A, Bissonnette B, Marchand J, Prince JC. Equipment for the analysis of the behaviour of concrete under restrained shrinkage at early ages. Magazine of Concrete Research. 2000;52(Compendex):297-302.

19. van Breugel K, de Vries H. Mixture Optimization of Low Water/Cement Ratio, High-Strength Concretes in View of Reduction of Autogenous Shrinkage. In: Aitcin P, Delagrave Y, editors. Proceedings International Symposium on High-Performance and Reactive Powder Concretes. University of Sherbrooke, Quebec, Canada1998. p. 365-82.
20. Bentz DP, Lura P, Weiss WJ. Reducing Early-Age Cracking in Concrete Today. West Lafayette, IN, Purdue University. 2008.
21. ASTM, Standard C 1581-04. Standard Test Method for Determining Age at Cracking and Induced Tensile Stress Characteristics of Mortar and Concrete under Restrained Shrinkage. ASTM International, West Conshohocken, PA Vol 4(2)2004. p. 787-92.
22. Moon J-H, Rajabipour F, Pease B, Weiss J. Quantifying the influence of specimen geometry on the results of the restrained ring test. Journal of ASTM International. 2006;3(8).
23. ACI Committee 207. 207.2R-07: Report on Thermal and Volume Change Effects on Cracking of Mass Concrete. American Concrete Institute2007.
24. Sant G, Lura P, Weiss J. Examining residual stress development in cementitious materials experiencing an early-age expansion. Proc, 9th CANMET-ACI Int Conf—TC Holland Symp. 2007:21–9.
25. Sant G, Rajabipour F, Weiss J. Examining Early Age Expansion In Pastes Containing Shrinkage Reducing Admixtures (SRA's). Advances in Concrete through Science and Engineering, RILEM Quebec. 2006:abstract p. 353 (electronic proceedings pp. 11).
26. Henkensiefken R, Bentz D, Nantung T, Weiss J. Volume change and cracking in internally cured mixtures made with saturated lightweight aggregate under sealed and unsealed conditions. Cement and Concrete Composites. 2009;31(7):427-37.
27. Lement BS, Averbach BL, Cohen M. The dimensional behavior of Invar. Invar Effect A Centennial Symposium Proceedings of an International Symposium on the Invar Effect held on the occasion of the 100th Anniversary of its Discovery, 7-8 Oct 1996. Warrendale, PA, USA: TMS; 1996. p. 171-96.
28. Guillaume CE. Invar and its applications. Nature. 1904.
29. Jacobs SF. Measuring Invar's dimensional stability. Invar Effect A Centennial Symposium Proceedings of an International Symposium on the Invar Effect held on the occasion of the 100th Anniversary of its Discovery, 7-8 Oct 1996. Warrendale, PA, USA: TMS; 1996. p. 157-69.
30. Nakamura Y. The Invar problem. IEEE Transactions on Magnetics. 1976;MAG-12(Copyright 1976, IEE):278-91.
31. Wittman F, Lukas J. EXPERIMENTAL STUDY OF THERMAL EXPANSION OF HARDENED CEMENT PASTE. 1974;7(Compendex):247-52.
32. Bjontegaard, Sellevold EJ. Thermal dilation-autogenous shrinkage: how to separate. In: Tazawa E, editor. Autogenous Shrinkage of Concrete: Proceedings of the Int Workshop organized by the JCI. Hiroshima1998.
33. Sellevold EJ, Bjontegaard. Coefficient of thermal expansion of cement paste and concrete: Mechanisms of moisture interaction. 293 ed. Van Godewijckstraat 30, Dordrecht, 3311, Netherlands: Springer Science and Business Media Netherlands; 2006. p. 809-15.
34. Vishay Measurements Group. Tech Note TN-505-4 'Strain Gage Selection Criteria Procedures Recommendations'. 2007.
35. Vishay Measurements Group. Instruction Bulletin B-127-14 'M-Bond -200 Installation Instructions'. 2008.
36. Vishay Measurements Group. Application Note VMM-19 'Surface Preparation'. 2005.
37. Vishay Measurements Group. Tech Note TN-504-1 'Strain Gage Thermal Output and Gage Factor Variation With Temperature'. 2007.
38. Hannah RL, Reed SE. Strain gage users' handbook1992.
39. Bentz DP, Snyder KA. Protected paste volume in concrete: Extension to internal curing using saturated lightweight fine aggregate. Cement and Concrete Research. 1999;29(11):1863-7.

40. ASTM, Standard C 1698-09. Standard Test Method for Autogenous Strain of Cement Paste and Mortar. ASTM International, West Conshohocken, PA2009.
41. Jensen OM, Hansen PF. Water-entrained cement-based materials: I. Principles and theoretical background. Cement and Concrete Research. 2001;31(4):647-54.
42. Bjontegaard, Hammer TA, Sellevold EJ. On the measurement of free deformation of early age cement paste and concrete. Cement and Concrete Composites. 2004;26(5):427-35.

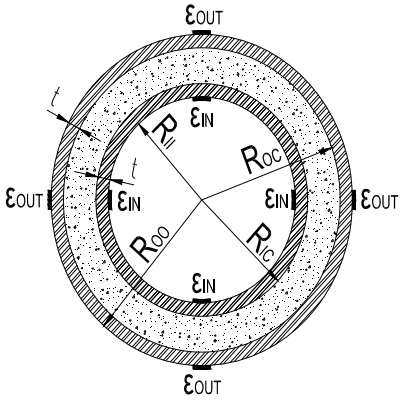

Figure 1 - Geometry of the Dual Ring Test

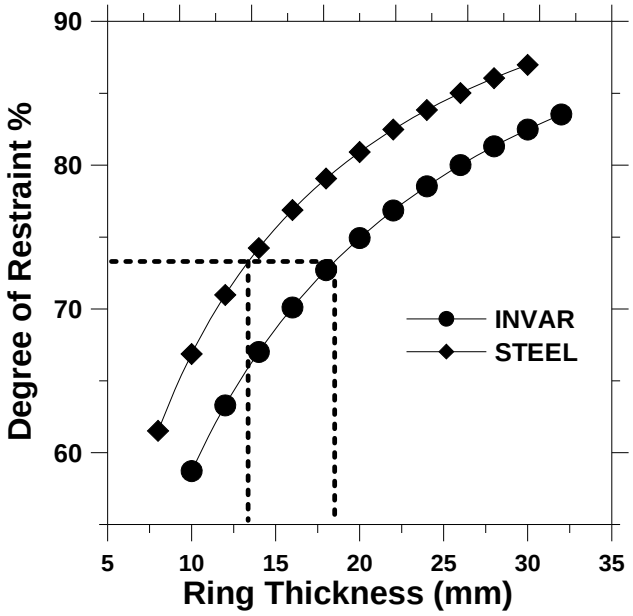

Figure 2 – Effect of Invar Ring Thickness on DOR

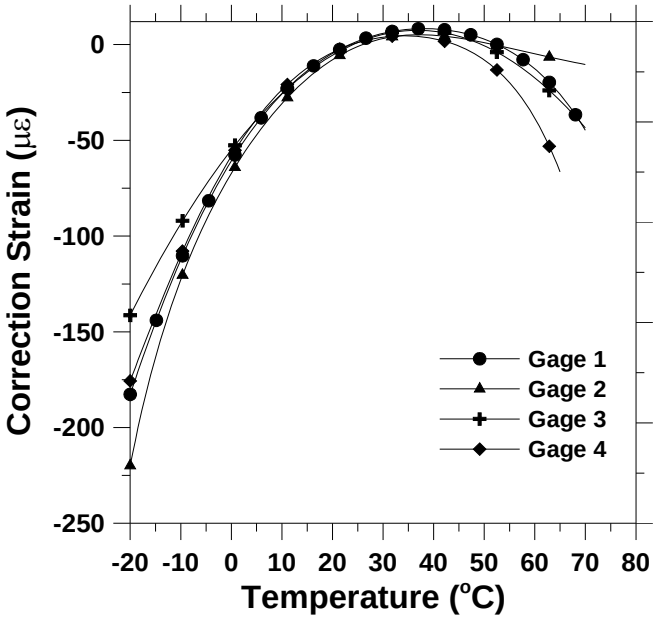

Figure 3a - Inner Ring Thermal Correction

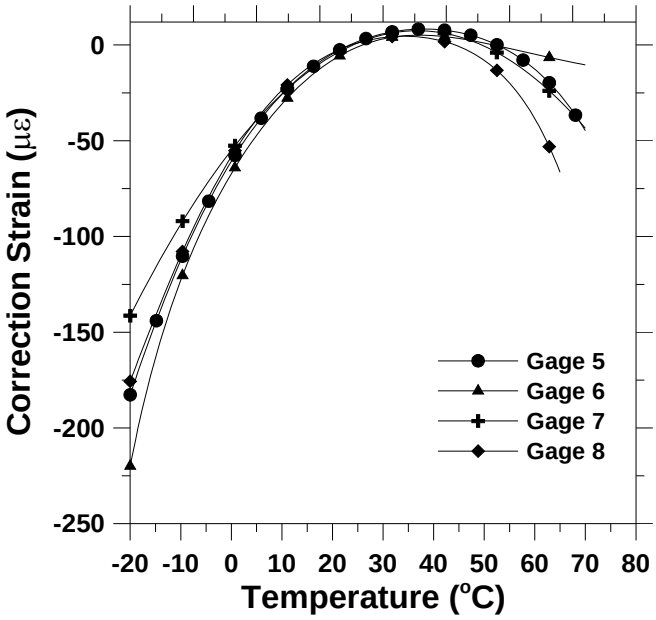

Figure 3b - Outer Ring Thermal Correction

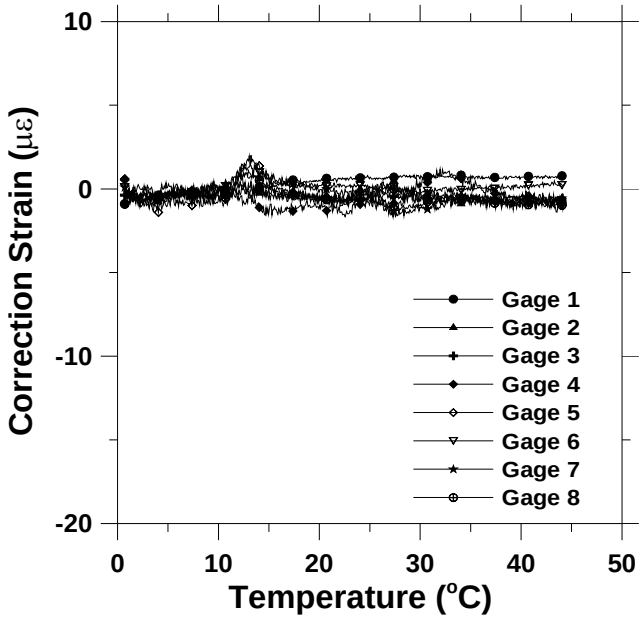

Figure 3c – Strain Thermal Corrections Verified

Figure 4a - Ring in insulation chamber with top insulation removed

552

553 *Figure 4b – Temperature regulation coil*

554

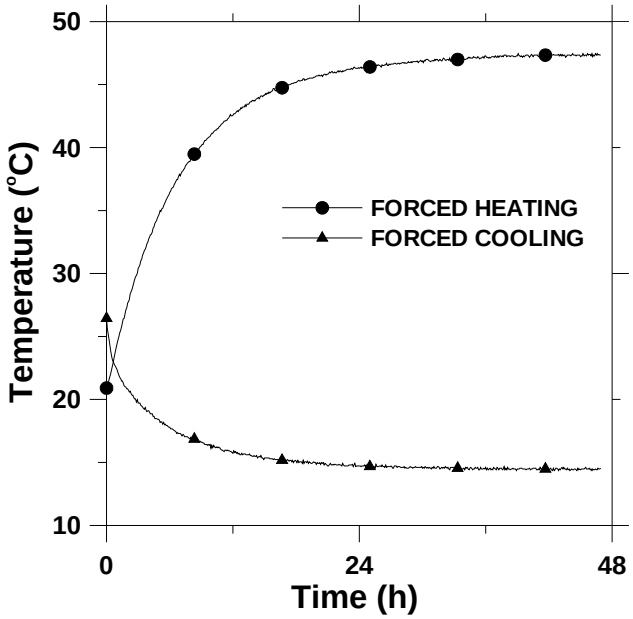

555

556 *Figure 5a - Forced Heating and Cooling Profile of Insulation Chamber*

557

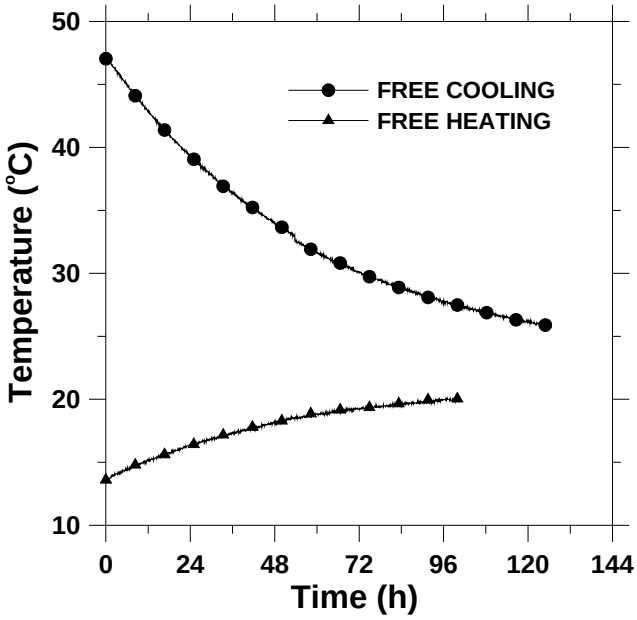

Figure 5b - Free heating and cooling profile of insulation chamber

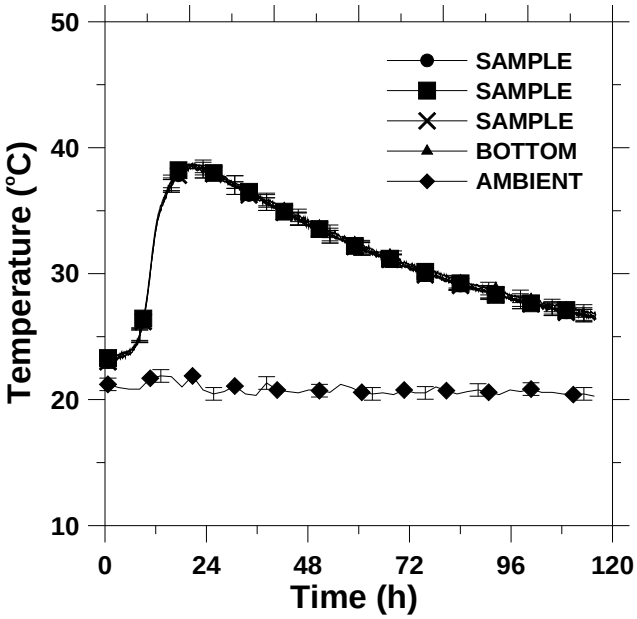

Figure 5c - Thermal Profile of Semi Adiabatic Plain Mortar

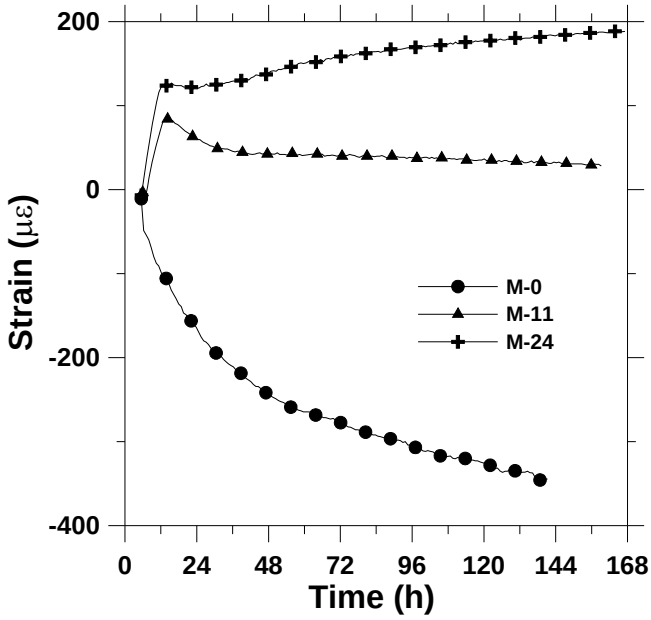

Figure 6 - Unrestrained Linear Autogenous Shrinkage

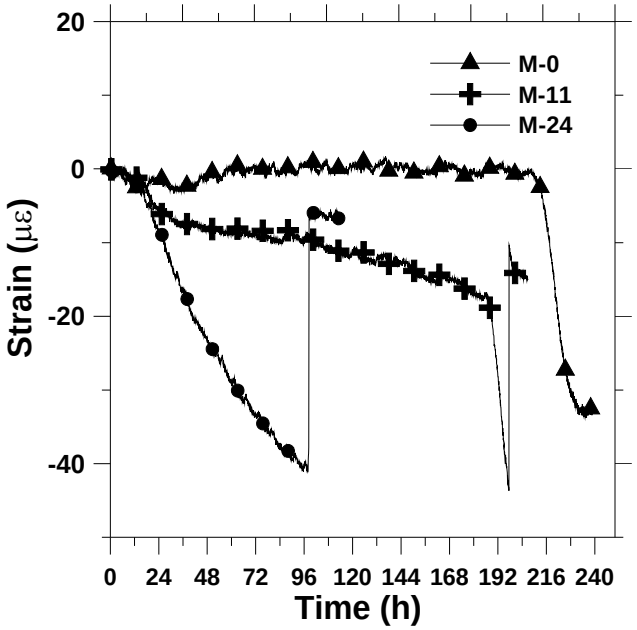

Figure 7a - Inner Ring Strain History

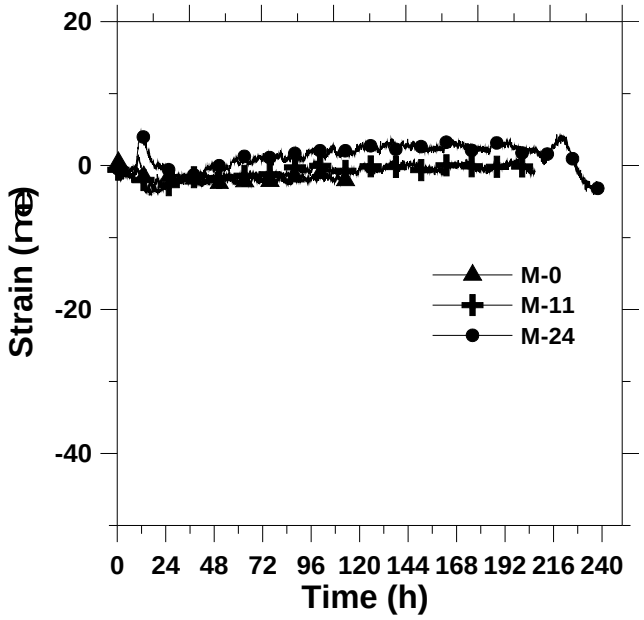

572

573 *Figure 7b – Outer Ring Strain History*

574

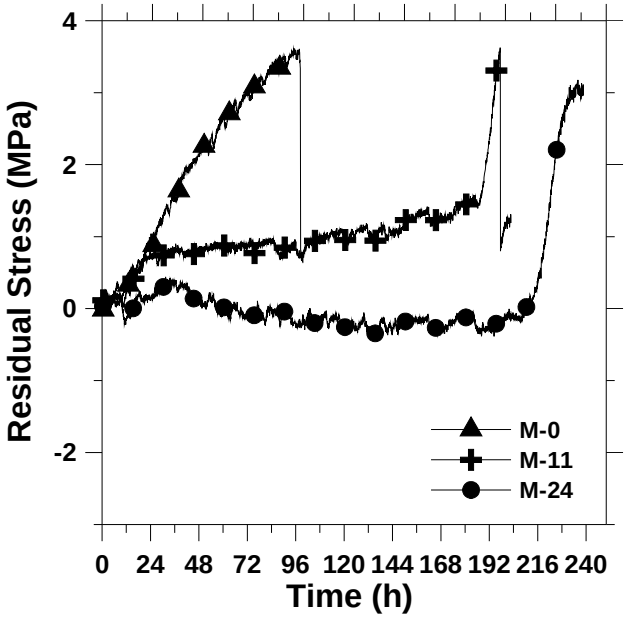

575

576 *Figure 8 – Residual Stress Development in Three Samples*

577

578